Optica Applicata, Vol. XLII, No. 4, 2012
DOI: 10.5277/oa120401

Plasmon excitation in periodic multilayers: modeling by boundary integral equations

ARNOŠT ŽÍDEK[1, *], JAROSLAV VLČEK[1, 2], JIŘÍ KRČEK[1]

[1]Department of Mathematics, VŠB – Technical University of Ostrava,
17. listopadu 15, 708 33 Ostrava-Poruba, Czech Republic

[2]Nanotechnology Centre, VŠB – Technical University of Ostrava,
17. listopadu 15, 708 33 Ostrava-Poruba, Czech Republic

[*]Corresponding author: arnost.zidek@vsb.cz

Optical diffraction is one of the few exploited applications of boundary integral equations. In this paper, a numerical model based on boundary integral equations (BIE) is applied to a periodic multilayer. We present possible implementations of a derived algorithm that enables solution, *e.g.*, for over-coated profiles. We give our attention to optical systems producing plasmon waves, for which we study the influence of several structural parameters on the diffraction response. The results are compared with the classical rigorous coupled waves method (RCWM) method, and, the case of non-smooth interface is discussed.

Keywords: optical diffraction, periodic multilayers, plasmon excitation, boundary integral method.

1. Introduction

Nano-patterned metals such as Au or Ag, which are used in many applications including in the design of optical devices and sensors based on surface plasmon resonance (SPR) [1, 2], draw great interest. There are two governing configurations permitting generation of an SP wave. The most frequent method works with coupling-based systems producing an evanescent wave by the total internal reflection (TIR) at the (planar) metal–dielectric interface in settlement with a coupling prism (Kretschmann or Otto set-up). Similarly, the evanescent field can lead to the rise of a SP wave, which comes up in the waveguide-based sensors at core–cladding interface. On the other hand, the diffraction at the surface of a metallic grating generates evanescent modes as the origin of SP excitation without prism or waveguide coupling. A rise of a SP wave results in reflection response from the optical system that can be observed as a dip in wavelength or angular spectrum of a reflected beam. Thus, the location, shape, depth or shift of this minimum can serve as detection phenomena used in a sensing device.

Besides more or less complicated experiments, theoretical studies are carried out including theoretical models of electromagnetic wave interaction with geometrically or materially modulated media. In the last three decades, numerous monographs and articles were published dealing with optical scattering, especially diffraction in periodic structures (*e.g.*, [3–5] and references therein). The various implementations of rigorous coupled waves method (RCWM) and differential method became the most frequently used [6–9]. One of relatively new approaches is based on boundary integral equations (BIE). The purely theoretical background of this method is referred to in [10–12] in the framework of optical diffraction, some typical applications can be found, including the papers [13–15]. The last approach appears very efficient, namely in the cases of more complicated profiles in optical multilayers, for which the other methods appear to be less suitable. The other advantage of the BIE method follows from the fact that only the amplitude coefficients at the boundaries of super- and superstrate are usually checked.

In this article, we aim to show a certain numerical model emerging from BIE applied on a periodic multilayer. We give our attention to optical systems producing plasmon waves, for which we study the influence of several structural parameters on the diffraction response. We introduce the main steps of an obtained algorithm and one of the possible implementations with numerical examples. The results are compared with the classical RCWM method, and the case of a non-smooth interface is discussed. Furthermore, we apply the algorithm on an over-coated profile, where we consider more than two different layers at the same height of the grating, but without any intersection of the boundaries. Finally, we present the method of BIE as an effective tool for solution of problems in plasmonic applications.

2. Boundary integral equations

2.1. Formulation of problem

We consider an optical structure of $(K-1)$ homogeneous layers divided by K periodically modulated boundaries with common period Λ in coordinate x_1 and uniform in the x_3 direction – see Fig. 1. In the single period we assume K smooth boundaries S_κ: $x_2 = f_\kappa(x_1)$, $x_1 \in [0, \Lambda]$, $\kappa = 1, 2, \ldots, K$ and two fictitious boundaries f_0: $x_2 = b_1 > \max(f_1)$ in the superstrate and f_{K+1}: $x_2 = -b_2 < \min(f_K)$ in the substrate. In such a way we generate a system of $(K+1)$ domains

$$\Omega^{(\kappa)} = \left\{ \left[x_1, x_2 \right] \in R^2, x_1 \in \left[0, \Lambda \right], f_{\kappa-1}(x_1) < x_2 < f_\kappa(x_1) \right\} \tag{1}$$

numbered from superstrate to substrate. At each boundary S_κ we introduce the unit normal vector $\mathbf{n}_\kappa$ as the inner one for $\Omega^{(\kappa)}$. Any layer is characterized by relative permittivity $\varepsilon^{(\kappa)}$ and relative permeability $\mu^{(\kappa)} = 1$.

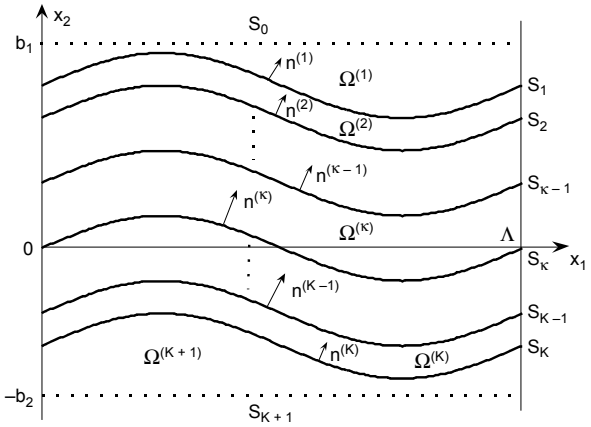

Fig. 1. Multilayer scheme with fictitious boundaries of the regions $\Omega^{(1)}$, $\Omega^{(\kappa+1)}$.

Incident monochromatic beam of wavelength λ propagates in the superstrate under incidence angle θ with respect to the x_2 axis in the plane $x_3 = 0$. The wave vectors are introduced as

$$\mathbf{k}^{(\kappa)} = \left(\alpha,\ \gamma^{(\kappa)},\ 0\right) \tag{2a}$$

$$\alpha = k_0\, n^{(1)} \sin(\theta) \tag{2b}$$

$$\left[k^{(\kappa)}\right]^2 = \left[k_0\, n^{(\kappa)}\right]^2 = \alpha^2 + \left[\gamma^{(\kappa)}\right]^2 \tag{2c}$$

where $n^{(\kappa)} = \sqrt{\varepsilon^{(\kappa)}\mu^{(\kappa)}}$ are the indices of refraction and $k_0 = 2\pi/\lambda$. As usual, we formulate the problem for basic polarizations of the incident beam. Thus, the spatially dependent complex factors of electromagnetic intensities have the form $\mathbf{E} = (0, 0, E_3)$, $\mathbf{H} = (H_1, H_2, 0)$ in the TE case or $\mathbf{E} = (E_1, E_2, 0)$, $\mathbf{H} = (0, 0, H_3)$ for TM field. Uniformity of interface in the x_3 coordinate allows us to write the problem as two-dimensional, where we denote $u(\mathbf{x}) = E_3(x_1, x_2)$ for TE or $u(\mathbf{x}) = H_3(x_1, x_2)$ for TM wave.

Being an interaction of light electromagnetic wave with material medium, optical diffraction is generally modeled by Maxwell equations with appropriate boundary conditions. The described situation allows us to consider the system of Helmholtz equations

$$\Delta u^{(\kappa)} + \left(k^{(\kappa)}\right)^2 u^{(\kappa)} = 0 \quad \text{in} \quad \Omega^{(\kappa)},\ \kappa = 1, ..., K+1 \tag{3}$$

with boundary conditions representing continuity of tangential field components on the smooth boundaries S_κ:

$$u^{(\kappa)} = u^{(\kappa+1)}, \qquad c_\kappa \frac{\partial u^{(\kappa)}}{\partial \mathbf{n}_\kappa} = \frac{\partial u^{(\kappa+1)}}{\partial \mathbf{n}_\kappa} \qquad \kappa = 1, ..., K \tag{4}$$

where $c_\kappa = 1$ for TE- and $c_\kappa = \varepsilon^{(\kappa+1)}/\varepsilon^{(\kappa)}$ for TM-polarized wave. The Sommerfeld radiation conditions ($x = \|\mathbf{x}\|$)

$$\lim_{x \to \infty} \sqrt{x} \left(\frac{\partial u^{(1)}}{\partial x} - ik^{(1)} u^{(1)} \right) = 0 \tag{5a}$$

$$\lim_{x \to -\infty} \sqrt{x} \left(\frac{\partial u^{(K+1)}}{\partial x} - ik^{(K+1)} u^{(K+1)} \right) = 0 \tag{5b}$$

are applied for far fields on fictitious boundaries S_0 and S_{K+1}. In the superstrate, the total field is expressed as the sum of incident and reflected field

$$u^{(1)}(\mathbf{x}) + u_{\text{in}}(\mathbf{x}), \qquad u_{\text{in}}(\mathbf{x}) = \exp\left[i \left(\alpha x_1 + \gamma_0^{(1+)} \right) x_2 \right] \tag{6}$$

Note that the function u_{in} describing a normalized incident wave on a zero diffraction order fulfills the Helmholtz equation in $\Omega^{(1)}$. The sign "+" in the superscript relates to a forward wave.

2.2. Integral representation

If we search for the solution of the Helmholtz equation $G(\mathbf{x}, \mathbf{y}) = G(\mathbf{x} - \mathbf{y})$ in a strip of the width Λ, for which the term $\exp(-i\alpha x_1)G$ is periodic in x_1 coordinate with period Λ, then the resulting quasi-periodic function has the form [16]

$$G(\mathbf{x}, \mathbf{y}) = \frac{1}{2i\Lambda} \sum_{m \in \mathbf{Z}} \frac{1}{\gamma_m} \exp\left\{ i \left[\alpha_m (x_1 - y_1) + \gamma_m |x_2 - y_2| \right] \right\} \tag{7}$$

where $\alpha_m = \alpha + 2\pi m/\Lambda$, $\gamma_m^2 = k^2 - \alpha_m^2$. The Green function (7) also satisfies Sommerfeld radiation conditions (5), but the series diverges for $(\mathbf{x} - \mathbf{y}) = \mathbf{o}$. Nevertheless, we are able to prove [17] that this singularity is of the logarithmical type, so that the difference $2\pi G(\mathbf{x} - \mathbf{y}) - \ln\|\mathbf{x} - \mathbf{y}\|$ is continuous for all $\mathbf{x}$, $\mathbf{y}$.

To formulate the scattering problem with the help of BIE, we start with the standard integral representation of the function $u^{(\kappa)}$ in arbitrary point $\mathbf{x} \in \Omega^{(\kappa)}$ by integrals along the boundary of the domain [18]. Because of periodicity and Sommerfeld conditions the computation is reduced only on the boundaries S_κ, $\kappa = 1, \ldots, K$.

As we first of all need to determine the fields and their normal derivatives on the boundaries, the limit transition $\mathbf{x} \in \Omega^{(\kappa)} \to \xi \in S_{\kappa-1} \cup S_\kappa$ must be realized in usual way. While the terms with kernel $G^{(\kappa)}(\mathbf{x}, \eta)$ are continuous on the interface, the potential of double layer has the jump of the size $\pm 0.5 u^{(\kappa)}(\xi)$, the sign of which corresponds to the normal orientation. We denote $v^{(\kappa)} = \partial u^{(\kappa)}/\partial \mathbf{n}$ and introduce the operators

$$V_{\lambda\mu}^{(\kappa)} v^{(\nu)} = 2 \int_{S_\mu} v^{(\nu)} G^{(\kappa)}(\xi_\lambda, \eta_\mu)\, \mathrm{d}l_\eta \tag{8a}$$

$$W_{\lambda\mu}^{(\kappa)} u^{(\nu)} = 2 \int_{S_\mu} u^{(\nu)} \frac{\partial G^{(\kappa)}(\xi_\lambda, \eta_\mu)}{\partial n_\mu}\, \mathrm{d}l_\eta \tag{8b}$$

thereby the upper indices relate to a layer and lower ones to actual boundaries. Since two limit processes come true toward the interfaces $S_{\kappa-1}$ or S_κ, we obtain two equations in any inner region $\Omega^{(\kappa)}$.

Finally, the application of boundary conditions (4) leads to the resulting system of boundary integral equations:

$$\begin{aligned}
u^{(1)}(\xi_1) &= -W_{1,1}^{(1)} u^{(1)} + V_{1,1}^{(1)} v^{(1)} - 2u_{\mathrm{in}}(\xi_1) \\
u^{(2)}(\xi_1) &= W_{1,1}^{(2)} u^{(1)} - c_1 V_{1,1}^{(1)} v^{(1)} - W_{1,2}^{(2)} u^{(2)} + V_{1,2}^{(2)} v^{(2)} \\
&\ldots \\
u^{(\kappa)}(\xi_\kappa) &= W_{\kappa,\kappa-1}^{(\kappa)} u^{(\kappa-1)} - c_{\kappa-1} V_{\kappa,\kappa-1}^{(\kappa)} v^{(\kappa-1)} - W_{\kappa,\kappa}^{(\kappa)} u^{(\kappa)} + V_{\kappa,\kappa}^{(\kappa)} v^{(\kappa)} \\
u^{(\kappa+1)}(\xi_\kappa) &= W_{\kappa,\kappa}^{(\kappa+1)} u^{(\kappa)} - c_\kappa V_{\kappa,\kappa}^{(\kappa+1)} v^{(\kappa)} - W_{\kappa,\kappa+1}^{(\kappa+1)} u^{(\kappa+1)} + V_{\kappa,\kappa+1}^{(\kappa+1)} v^{(\kappa+1)} \\
&\ldots \\
u^{(K)}(\xi_K) &= W_{K,K-1}^{(K)} u^{(K-1)} - c_{K-1} V_{K,K-1}^{(K)} v^{(K-1)} - W_{K,K}^{(K)} u^{(K)} + V_{K,K}^{(K)} v^{(K)} \\
u^{(K+1)}(\xi_K) &= W_{K,K}^{(K+1)} u^{(K)} - c_K V_{K,K}^{(K+1)} v^{(K)}
\end{aligned} \tag{9}$$

Considering $u^{(K+1)} = u^{(K)}$ in the last equation, we obtained a $2K$-dimensional problem for the same number of unknown functions $u^{(\kappa)}$, $v^{(\kappa)}$, $\kappa = 1, 2, \ldots, K$, so that the solution will be unique. Obviously, the fields $u^{(K+1)}$, $v^{(K+1)}$ follow from boundary conditions on the last interface.

2.3. Reflectance and transmittance

These parameters serve as basic characteristics of an optical system for the given angle of incidence and wavelength. We will determine them using diffraction coefficients ρ_m and τ_m of reflected and transmitted modes. They correspond to the coefficients of Rayleigh expansion of the planar optical beam in the semi-infinite regions outside the multilayer:

$$u^{(1)}(\mathbf{x}) = \sum_{m \in \mathbf{Z}} \rho_m^{(1-)} \exp\left[i\left(\alpha_m x_1 + \gamma_m^{(1-)} x_2 \right) \right], \quad x_2 > b_1 > 0 \tag{10}$$

$$u^{(K+1)}(\mathbf{x}) = \sum_{m \in \mathbf{Z}} \tau_m^{(K+1)} \exp\left[i\left(\alpha_m x_1 + \gamma_m^{(K+1+)} x_2 \right) \right], \quad x_2 < -b_2 < 0 \tag{11}$$

Together we can represent these fields by integral formulas including boundary conditions, so that we can calculate amplitude coefficients of the arbitrary mode in the integral form comparing both representations at any diffraction order. Finally, the reflectance R_m and transmittance T_m of the m-th mode are real characteristics defined as

$$R_m = \left| \rho_m^{(1-)} \right|^2 \frac{\mathrm{Re}\left(\gamma_m^{(1-)} \right)}{\mathrm{Re}\left(\gamma_m^{(1+)} \right)} \tag{12a}$$

$$T_m = \left| \frac{\tau_m^{(K+1)}}{c_K} \right|^2 \frac{\mathrm{Re}\left(\gamma_m^{(K+1+)} \right)}{\mathrm{Re}\left(\gamma_0^{(1+)} \right)} \tag{12b}$$

3. Numerical solution

3.1. Parametrization

Let $\mathbf{p}_\mu(t) = (p_{\mu 1}(t), p_{\mu 2}(t)), t \in [0, 2\pi], \nu = 1, \ldots, K$ be a parametrization of the boundary S_μ. Thus, we have $\eta_\mu = \mathbf{p}_\mu(t), t \in [0, 2\pi]$ with normal vector

$$\mathbf{n}_\mu(t) = (-\dot{p}_{\mu 2}(t), \dot{p}_{\mu 1}(t)), \qquad \left\| \mathbf{n}_\mu \right\| = n_\mu(t) = \sqrt{\dot{p}_{\mu 1}^2 + \dot{p}_{\mu 2}^2} \tag{13}$$

In the integral operators, the points ξ, η can lie on the same boundary or on different neighboring interfaces S_λ, S_μ. Therefore, the periodical Green function (7) need be written as

$$G^{(\kappa)}(s, t) = \sum_{m \in \mathbf{Z}} G_m^{(\kappa)}(\mathbf{p}_\lambda(s), \mathbf{p}_\mu(t)) \tag{14}$$

If $\lambda = \mu$, nothing but kernels of the operators $V_{\mu\mu}^{(\kappa)}$ and $W_{\mu\mu}^{(\kappa)}$ exhibit singularity in the system (9). The operator $W_{\mu\mu}^{(\kappa)}$ remains continuous on the boundary [19] assuming that the parametrization used is twice differentiable. In the operator $V_{\mu\mu}^{(\kappa)}$ the logarithmical term can be expressed by harmonic series

$$\ln \left\| p_\mu(s) - p_\mu(t) \right\| = \sum_{m \neq 0} \frac{\exp\left[-im(s-t) \right]}{2|m|} \tag{15}$$

being unchanged in all layers $\Omega^{(\kappa)}$ [17]. Thus, the singular kernel of operator $V_{\mu\mu}^{(\kappa)}$ must be split as follows:

$$G^{(\kappa)}(s,t) = G_0^{(\kappa)}(s,t) + \sum_{m\neq 0}\left\{ G_m^{(\kappa)}(s,t) - \frac{1}{2\pi}\frac{\exp\left[-im(s-t)\right]}{2|m|}\right\} + \\ + \frac{1}{2\pi}\sum_{m\neq 0}\frac{\exp\left[-im(s-t)\right]}{2|m|} \tag{16}$$

Correspondingly we write the single layer operator as the sum $V_{\mu\mu}^{(\kappa)} = K_{\mu\mu}^{(\kappa)} + L$, because the first two right-hand side terms of (16) represent the kernel of the compact operator $K_{\mu\mu}^{(\kappa)}$, and, the last one is the kernel of the singular operator L.

3.2. Discretization

We can use several methods that differ by the accuracy or by suitability for a given problem. Among many published resources we briefly mention the monograph [20], which covers the problems of electromagnetism. Here, we will exploit an implementation of the collocation method [21]. We choose $(2N+1)$ equidistant collocation points from the interval $[0, 2\pi]$ on all the boundaries S_κ, so that $s_j = 2\pi j/(2N+1)$, $j = 0, 1, \ldots, 2N$. Further, we represent the functions $u^{(\kappa)}$ and $v^{(\kappa)}$ on the interval $[0, 2\pi]$ with respect to the trigonometric interpolation basis of functions

$$\phi_n(t) = \frac{1}{2N+1}\sum_{l=-N}^{N}\exp\left(-\frac{2\pi i n l}{2N+1}\right)\exp(ilt), \qquad n = 0, 1, 2, \ldots, 2N \tag{17}$$

as the linear combinations

$$u^{(\kappa)}(t) = \sum_{n=0}^{2N} u_n^{(\kappa)}\phi_n(t) \tag{18a}$$

$$v^{(\kappa)}(t) = \sum_{n=0}^{2N} v_n^{(\kappa)}\phi_n(t) \tag{18b}$$

It can be easily proven that $\phi_n(s_j) = \delta_{nj}$, therefore, the coefficients of series are exactly equal to the values in collocation points, *i.e.*, $u^{(\kappa)}(s_n) = u_n^{(\kappa)}$, $v^{(\kappa)}(s_n) = v_n^{(\kappa)}$.

3.3. Numerical integration

Generally, a computation of integrals uses quadrature rules; however, we can exploit the simple trapezoidal method with sufficient accuracy. We choose again $(2N+1)$ points $t_k = 2\pi k/(2N+1)$, $k = 0, 1, \ldots, 2N$ in the integration interval, so that the computation scheme (*e.g.*, for a functional W applied to periodical function u) has the form

$$W_{\lambda\mu}^{(\kappa)} u_n^{(v)}(s_j, t) = 2\int_0^{2\pi} u^{(v)}(t)\mathbf{n}_\mu(t) \cdot \nabla G^{(\kappa)}(s_j, t)\mathrm{d}t \approx \sum_{k=0}^{2N} W_{\lambda\mu, jk}^{(\kappa)} u_k^{(v)} \tag{19}$$

$$W_{\lambda\mu, jk}^{(\kappa)} = \frac{4\pi}{2N+1} u^{(v)}(t_k)\mathbf{n}_\mu(t_k) \cdot \nabla G^{(\kappa)}\Big(\mathbf{p}_\lambda(s_j), \mathbf{p}_\mu(t_k)\Big) \tag{20}$$

Using the decomposition (16), we similarly obtain for the second operator with regular kernel

$$K_{\lambda\mu}^{(\kappa)} = V_\kappa^{(\kappa)} - L \tag{21a}$$

$$K_{\lambda\mu}^{(\kappa)} v^{(v)}(s_j, t) \approx \sum_{k=0}^{2N} K_{\lambda\mu, jk}^{(\kappa)} v_k^{(v)} \tag{21b}$$

Analytical calculation of the singular operator L consists in direct analytical integration,

$$Lv^{(\kappa)}(s_j, t) \approx \sum_{k=0}^{2N} L_{jk} v_k^{(\kappa)} \tag{22a}$$

$$L_{jk} = \sum_{\substack{l=-N \\ l\neq 0}}^{N} \frac{1}{|l|} \exp\left[\frac{2\pi i l(j-k)}{2N+1}\right] \tag{22b}$$

Obtained results allow us to transform the system (9) into an algebraic problem for unknown values of the fields $u^{(\kappa)}$ and $v^{(\kappa)}$ in collocation points. We write this one in a matrix form

$$\mathbf{A} \cdot \mathbf{w} = \mathbf{b} \tag{23a}$$

$$\mathbf{w} = \left[\mathbf{u}^{(1)} \ \mathbf{v}^{(1)} \ \ldots \ \mathbf{u}^{(K)} \ \mathbf{v}^{(K)}\right]^T \tag{23b}$$

$$\mathbf{b} = \left[-2\mathbf{u}_{\mathbf{in}} \ \mathbf{o} \ \ldots \ \mathbf{o}\right]^T \tag{23c}$$

where the matrix $\mathbf{A}$ is block-wise structured with the sub-matrices ($\kappa = 2, \ldots, K$)

$$\mathbf{A}_1^{(1)} = \left[\mathbf{W}_{1,1}^{(1)} + \mathbf{I} \quad \mathbf{V}_{1,1}^{(1)}\right] \tag{24a}$$

$$\mathbf{A}_K^{(K+1)} = \left[-\mathbf{W}_{K,K}^{(K+1)} + \mathbf{I} \quad c_k(\mathbf{K}_{K,K}^{(K+1)} + \mathbf{L})\right] \tag{24b}$$

$$\mathbf{A}_{\kappa-1}^{(\kappa)} = \begin{bmatrix} -\mathbf{W}_{\kappa-1,\,\kappa-1}^{(\kappa)} & c_{\kappa-1}(\mathbf{K}_{\kappa-1,\,\kappa-1}^{(\kappa)} + \mathbf{L}) \\ \mathbf{W}_{\kappa,\,\kappa-1}^{(\kappa)} & c_{\kappa-1}\mathbf{V}_{\kappa,\,\kappa-1}^{(\kappa)} \end{bmatrix} \tag{24c}$$

$$\mathbf{A}_{\kappa}^{(\kappa)} = \begin{bmatrix} \mathbf{W}_{\kappa-1,\,\kappa}^{(\kappa)} + \mathbf{I} & -\mathbf{V}_{\kappa-1,\,\kappa}^{(\kappa)} \\ \mathbf{W}_{\kappa,\,\kappa}^{(\kappa)} + \mathbf{I} & -(\mathbf{K}_{\kappa,\,\kappa}^{(\kappa)} + \mathbf{L}) \end{bmatrix} \tag{24d}$$

The matrix elements are computed by formulas (21–23) thereby **I** and **o** denote the identity and zero matrices, respectively. Further, **u**, **v** and $\mathbf{u_{in}}$ are the $(2N + 1)$-dimensional vectors containing coefficients of the series (18).

3.4. The case of non-smooth boundary

The presented algorithm is based on the assumption that the normal vector exists in any point of interface. If this condition does not hold, the further steps depend on the disturbance type. In many cases, this fact can be expressed analytically through limit transition of the boundary [18]. The more sophisticated way consists in the introducing especial functions spaces and operators over them [10]. On the other hand, it suffices in some practical computations to care so that the collocation point does not fall into singularity on the boundary.

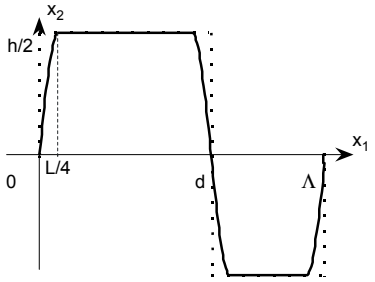

◀ Fig. 2. A smoothing of binary profile.

Here, we propose a smoothing of boundary profile to compensate points with a non-existing normal vector. We will demonstrate this idea for the rectangular binary profile – see Fig. 2. In the neighborhood of the corners, we replace the part containing a jump by one quarter of the period of the function sinus with appropriately chosen properties. Thus, the smoothing function can be written as $0.5h\sin(2\pi x_1/L)$, where h is the profile height, and, the period $L < \Lambda$ satisfies the conditions $L/2 < \mathrm{d}$, $L/2 < \Lambda - d$ with d denoting the width of the lamel. The parametrization $\mathbf{p}(t) = (p_1(t), p_2(t))$, $t \in [0, 2\pi]$ of the smoothed profile takes the form

$$p_1(t) = \frac{\Lambda}{2\pi} t \tag{25a}$$

$$p_2(t) = \frac{h}{2}\begin{cases} \sin\left(\dfrac{\Lambda}{L}t\right), & t \in \left[0, \dfrac{\pi L}{2\Lambda}\right] \\ 1, & t \in \left[\dfrac{\pi L}{2\Lambda}, \dfrac{2\pi}{\Lambda}\left(d - \dfrac{L}{4}\right)\right] \\ -\sin\left[\dfrac{\Lambda}{L}\left(t - \dfrac{2\pi d}{\Lambda}\right)\right], & t \in \left[\dfrac{2\pi}{\Lambda}\left(d - \dfrac{L}{4}\right), \dfrac{2\pi}{\Lambda}\left(d + \dfrac{L}{4}\right)\right] \\ -1, & t \in \left[\dfrac{2\pi}{\Lambda}\left(d + \dfrac{L}{4}\right), \dfrac{2\pi}{\Lambda}\left(\Lambda - \dfrac{L}{4}\right)\right] \\ \sin\left[\dfrac{\Lambda}{L}(t - 2\pi)\right], & t \in \left[\dfrac{2\pi}{\Lambda}\left(\Lambda - \dfrac{L}{4}\right), 2\pi\right] \end{cases} \tag{25b}$$

It can be easily proven that this parametrization is differentiable in the link-up points. Note that the described approach can be extended for other profiles and smoothing functions.

4. Results and discussion

4.1. BIE vs. RCWM

The described computing scheme was implemented in MATLAB code and tested at first for the sine boundary between air ($\varepsilon^{(1)} = 1$) and glass (SiO_2, $\varepsilon^{(2)} = 2.25$) on the wavelength $\lambda = 632.8$ nm. The period Λ and depth h of the interface were chosen as 300 nm and 24 nm, respectively. The highest considered diffraction order $N = 24$ was equal to the discretization factor, and therefore 49 collocation points. The results were successfully compared to the data obtained by the RCWM with 20 parallel binary sub-layers and the same number of diffraction orders. The reflectance and transmittance data for both basic polarizations by the incidence angle 45° and diffraction orders 0 and –1 are summarized in Tab. 1. We could obtain better agreement with the benchmark using more effective quadrature rules for computation of integrals instead of the trapezoidal method.

T a b l e 1. The results comparison of two computational models.

	Reflectance R_s		Transmittance T_s		Reflectance R_p		Transmittance T_p	
N	BIE	RCWM	BIE	RCWM	BIE	RCWM	BIE	RCWM
–1	0	0	0.0015	0.0016	0	0	0.0012	0.0011
0	0.0900	0.0900	0.9088	0.9083	0.0083	0.0083	0.9907	0.9906

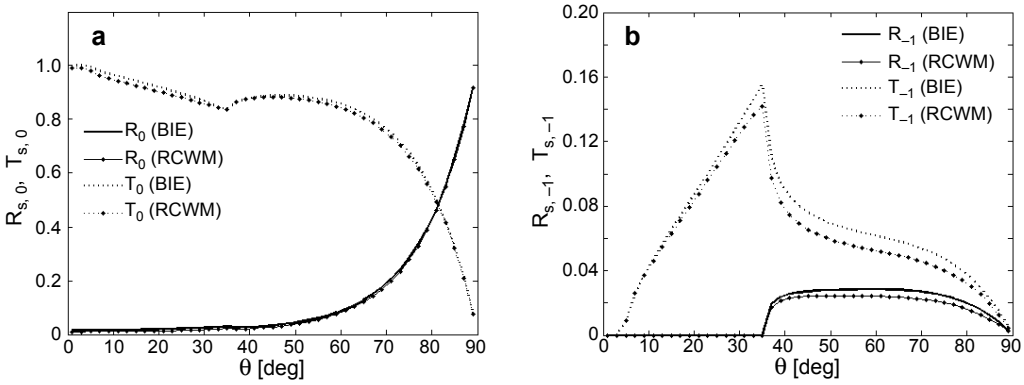

Fig. 3. A comparison of BIE algorithm to RCWM (the highest discretization order $N = 35$) for the diffraction orders 0 (**a**) and –1 (**b**).

In order to ascertain the smoothing effect, we modeled diffraction response from lamellar grating with period $\Lambda = 400$ nm, height $h = 120$ nm and width of lamellas 200 nm. Figure 3 shows the reflectance and transmittance at the diffraction orders 0 and –1 calculated for *s*-polarized incident wave using the rigorous coupled wave method and by the presented BIE algorithm with sine smoothing ($L = 140$ nm). Also, the alternative simulation showed satisfactory agreement of both methods even for a quite broad testing interval of the period L from 80 to 200 nm. Obviously, the degree of discretization must be increased for lower values of L that adversely influences the accuracy of results. On the other hand, a widening of the smoothing period leads to the loss of the binary character of grating.

4.2. Multilayers with plasmonic response

The first example demonstrates the system "coupling prism/Au grating/air" in Fig. 4 where the incident *p*-polarized beam ($\lambda = 632.8$ nm) propagates from prism (BK7 glass, $\varepsilon = 1.5146$ [22]) into gold grating ($\varepsilon = 0.1911 + 3.3577i$ [23]). With regard to the total internal reflection, the developed evanescent field excites the surface plasmon wave that is diffracted on the following periodically modulated interface. We compared the reflection response from the pure sine grating and from a binary one of the same period $\Lambda = 480$ nm and the depth $h = 20$ nm. In both models, the average thickness of the gold nano-layer was $T = 20$ nm. The graphs in Fig. 4 validate an expectation of SPR response flattening due to an increase of the smoothing period.

The largest diffraction order $N = 35$ implies 71 collocation points with the distance of less than 7 nm from the neighboring pair in this numerical task. Among other things, it means that the shortest smoothing period of 48 nm practically preserves the binary profile. Note, that for the use of derived trapezoidal integration scheme in the case of smooth profiles it is sufficient to adapt the number $(2N + 1)$ of collocation points to the grating period Λ so as $N \sim \Lambda/20$.

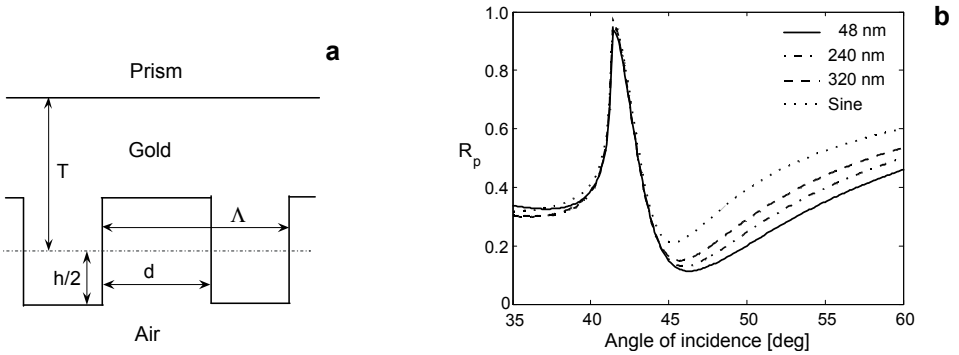

Fig. 4. Surface plasmon excitation in binary coupling system ($N = 35$, diffraction order 0). Binary grating scheme (**a**). Reflectance by increasing period of smoothing L (**b**).

In the next group of numerical tests we simulated the dependence of plasmonic response on such governing geometrical parameters as grating period or depth of groves. We modeled the same diffraction system as in the previous application, however with smooth sine interface gold–air (Fig. 5**a**).

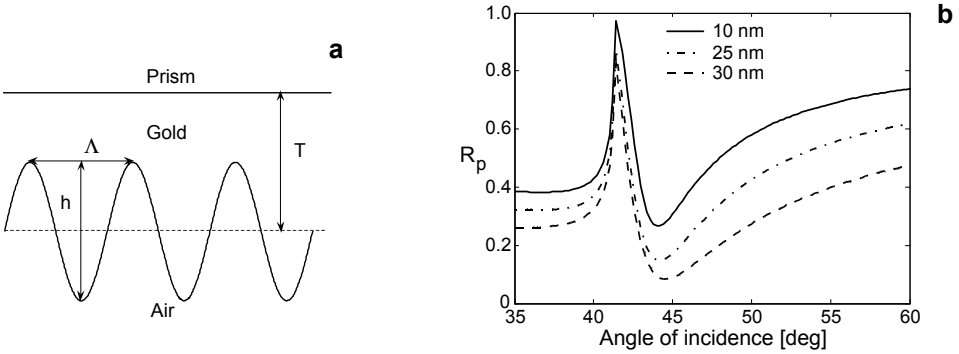

Fig. 5. Surface plasmon excitation in a smooth periodical coupling system (sine profile, $N = 15$). Grating scheme (the thickness $T = 15$ nm fixed) (**a**). Reflectance by increasing grove depth h (**b**).

The reflectance for a light beam propagating from prism to grating exhibits, at a zero diffraction order, the SPR response illustrated in Figs. 5**b** and 6**a**. In both cases, we fixed the averaged thickness $T = 15$ nm of the gold nano-layer. Figure 5**b** demonstrates simultaneous increased depth of resonance dips and the boundary profile height by the preserved grating period $\Lambda = 350$ nm. Especially, the last value $h = 30$ nm means that the periodic profile attains the planar interface prism–gold.

If the period of grating Λ is close to incident field wavelength $\lambda = 632.8$ nm, the SPR effect becomes very expressive. This fact is illustrated in Fig. 6**a** by fixed depth of groves $h = 20$ nm. In practice, the described properties have an indispensable role in sensing the elements design based on the SPR effect.

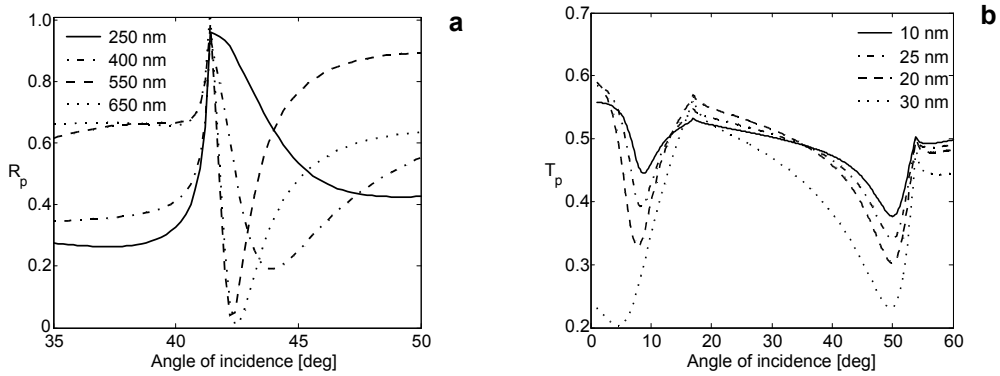

Fig. 6. SPR in the system as in the Fig. 5**a** – the dependence on grating period Λ ($T = 15$ nm, $h = 20$ nm) (**a**). Localized SPR by opposite propagation direction – dependence on the depth h ($T = 15$ nm, $\lambda = 350$ nm) (**b**).

A profoundly different situation occurs if the light beam propagates through the introduced structure in the opposite direction. The optical coupling does not occur due to the total internal reflection, however, the plasmon generation can also be reached in the form of a pair of so-called localized plasmons. This result is clearly presented in Fig. 6**b**, again for the grating period 350 nm. Obviously, the character of response is predetermined by the geometrical attributes of the grating as well. One of typical cases is demonstrated in Fig. 6**b** for the transmitted field. Similarly as in the example 5**b**, we modeled an influence of the varying depth of the grating profile, and thereby its period 350 nm remains unchanged. We can also see that a change of grove height influences the angular position of the resonant state excited only for the low incidence angles.

The method of BIE offers significant advantage in the diffraction problems characterized by over-coated interfaces, for which the other techniques are not appli-

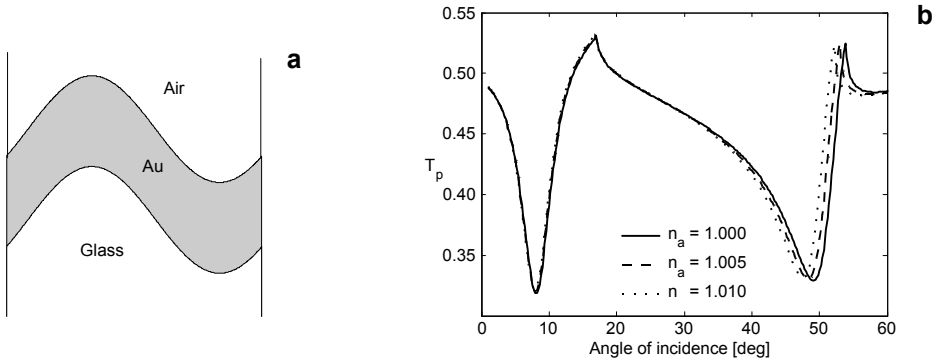

Fig. 7. A couple of over-coated sine profiles (**a**). Transmittance by changing refraction index n_a of ambient ($T = 15$ nm, $\Lambda = 350$ nm, $h = 20$ nm, $N = 15$) (**b**).

cable (RCWM) or bring realization troubles. In the last example we illustrate the computational ability of a derived algorithm for a double of sine profiles (Fig. 7**a**). In this case, we emphasize the sensitivity of optical SPR systems to very small variations in the optical function of ambience that is usually an exploited feature in sensing element design.

We modeled the situation when the incoming beam propagates from air superstrate. As we can see in Fig. 7**b**, the successive increase of the refraction index with the step $\Delta n_a = 0.005$ gives rise to a pronounced angular shift of resonance minima. This one is more expressive for larger angles of incidence, for which the influence of air–Au interface prevails.

5. Conclusions

We have presented a numerical study of the optical response from a periodically modulated lamellar grating. As a theoretical tool, the method of boundary integral equations was used that enables a solution for relatively general types of periodic interfaces to be found. We showed an implementation for an optical multilayer; moreover, we proposed an analytical smoothing of a general profile that enables sufficient accuracy.

We validated the applicability of the introduced computational scheme to the effects leading to plasmon excitation for both principal cases, *i.e.*, surface plasmons generated in a prism-coupling system (in Kretschmann configuration) or localized plasmons in a metallic grating on a dielectric substrate. We demonstrated in which manner the structural parameters of a periodic nano-layer modify diffraction response. Obtained results confirm the promising potential of using BIE in a variety of optical applications.

Acknowledgements – This work has been partially supported by the IT4 Innovations Centre of Excellence Project, reg. no. CZ.1.05/1.1.00/02.0070.

References

[1] HOMOLA J., YEE S.S., GAUGLITZ G., *Surface plasmon resonance sensors: review*, Sensors and Actuators B: Chemical **54**(1–2), 1999, pp. 3–15.

[2] HUTTER E., FENDLER J.H., *Exploitation of localized surface plasmon resonance*, Advanced Materials **16**(19), 2004, pp. 1685–1706.

[3] PETIT R., [ED.], *Electromagnetic Theory of Gratings*, Springer, Berlin, 1980.

[4] NEVIÈRE M., POPOV E., *Light Propagation in Periodic Media: Differential Theory and Design*, Marcel Dekker, New York, 2002.

[5] BAO G., COWSAR L., MASTERS W., [EDS.], *Mathematical Modeling in Optical Science*, SIAM, Philadelphia, 2001.

[6] GLYTSIS E.N., GAYLORD T.K., *Rigorous three-dimensional coupled-wave diffraction analysis of single and cascaded anisotropic gratings*, Journal of the Optical Society of America A **4**(11), 1987, pp. 2061–2080.

[7] LIFENG LI, *Formulation and comparison of two recursive matrix algorithms for modeling layered diffraction gratings*, Journal of the Optical Society of America A **13**(5), 1996, pp. 1024–1035.

[8] GRANET G., GUIZAL B., *Efficient implementation of the coupled wave method for metallic lamellar gratings in TM polarization*, Journal of the Optical Society of America A **13**(5), 1996, pp. 1019–1023.
[9] POPOV E., NEVIÈRE M., *Differential theory for diffraction gratings: a new formulation for TM polarization with rapid convergence*, Optics Letters **25**(9), 2000, pp. 598–600.
[10] COSTABEL M., STEPHAN E., *A direct boundary integral equation method for transmission problems*, Journal of Mathematical Analysis and Applications **106**(2), 1985, pp. 367–413.
[11] NEDELEC J.C., STARLING F., *Integral equation methods in a quasi-periodic diffraction problem for the time-harmonic Maxwell's* equations, SIAM Journal on Mathematical Analysis **22**(6), 1991, pp. 1679–1701.
[12] ELSCHNER J., SCHMIDT G., *Diffraction in periodic structures and optimal design of binary gratings. Part I: Direct problems and gradient formulas*, Mathematical Methods in the Applied Sciences **21**(14), 1998, pp. 1297–1342.
[13] PRATHER D.W., MIROTZNIK M.S., MAIT J.N., *Boundary integral methods applied to the analysis of diffractive optical elements*, Journal of the Optical Society of America A **14**(1), 1997, pp. 34–43.
[14] BENDICKSON J.M., GLYTSIS E.N., GAYLORD T.K., PETERSON A.F., *Modeling considerations of rigorous boundary element method analysis of diffractive optical elements*, Journal of the Optical Society of America A **18**(7), 2001, pp. 1495–1506.
[15] MAGATH T., SEREBRYANNIKOV A.E., *Fast iterative, coupled-integral-equation technique for inhomogeneous profiled and periodic slabs*, Journal of the Optical Society of America A **22**(11), 2005, pp. 2405–2418.
[16] LINTON C.M., *The Green's function for the two-dimensional Helmholtz equation in periodic domains*, Journal of Engineering Mathematics **33**(4), 1998, pp. 377–401.
[17] ŽÍDEK A., VLČEK J., KRČEK J., *Solution of diffraction problems by boundary integral equations*, Proceedings of 11th International Conference APLIMAT 2012, February 7–9, 2012, Bratislava, Slovak Republic, publ. by Faculty of Mechanical Engineering, Slovak University of Technology, Bratislava, 2012, pp. 221–229.
[18] PARÍS F., CAÑAS J., *Boundary Element Method. Fundamentals and Applications*, Oxford Univesity Press, Oxford, 1997.
[19] DOBSON D., FRIEDMANN A., *The Time-Harmonic Maxwell Equations in a Doubly Periodic Structure*, www.ima.umn.edu/preprints/Feb91Series/762.pdf
[20] PEI-BAI ZHOU, *Numerical Analysis of Electromagnetic Fields*, Springer Verlag, Berlin, 1993.
[21] KLEEMANN B.H., MITREITER A., WYROWSKI F., *Integral equation method with parametrization of grating profile. Theory and experiments*, Journal of Modern Optics **43**(7), 1996, pp. 1323–1349.
[22] www.sciner.com/Opticsland/FS.htm
[23] JOHNSON P.B., CHRISTY R.W., *Optical constants of the noble metals*, Physical Review B **6**(12), 1972, pp. 4370–4379.

Received March 14, 2012
in revised form May 24, 2012